# Localization of Metastable Atom Beams with Optical Standing Waves: Nanolithography at the Heisenberg Limit

K. S. Johnson,* J. H. Thywissen, N. H. Dekker, K. K. Berggren,† A. P. Chu,‡ R. Younkin, M. Prentiss

The spatially dependent de-excitation of a beam of metastable argon atoms, traveling through an optical standing wave, produced a periodic array of localized metastable atoms with position and momentum spreads approaching the limit stated by the Heisenberg uncertainty principle. Silicon and silicon dioxide substrates placed in the path of the atom beam were patterned by the metastable atoms. The de-excitation of metastable atoms upon collision with the surface promoted the deposition of a carbonaceous film from a vapor-phase hydrocarbon precursor. The resulting patterns were imaged both directly and after chemical etching. Thus, quantum-mechanical steady-state atom distributions can be used for sub-0.1-micrometer lithography.

Several nanolithography techniques rely on the use of energetic particles (such as photons, ions, or electrons) to initiate alterations (such as etching or chemical reactions) over regions of a surface selected with physical masks. Neutral metastable atoms have also been explored as an alternative source; the use of such atoms avoids electrostatic interactions that can limit the resolution of patterning with charged particles, and their low kinetic energies cause little damage to the substrate material. We have used metastable argon (Ar*) atoms (*1*) to pattern substrates in the presence of a hydrocarbon vapor. The release of energy (~12 eV) into these hydrocarbon molecules (*2*) produces a durable carbonaceous material that has excellent resistance to several wet and dry chemical etches and can be used to transfer patterns into Au, Si, $SiO_2$ (*3*, *4*), and GaAs (*5*) with feature sizes as small as 20 nm (*4*). Previous experiments have used metastable atom beams to damage self-assembled monolayers of alkanethiolates on gold films, demonstrating pattern transfer with edge resolutions of less than 100 nm (*6*).

The use of physical masks is limiting in several ways. Free-standing stencil masks may clog and must be positioned very close to the substrate to minimize the spreading of the particle beam during free flight. Additionally, the mechanical stability and structural integrity requirements of free-standing masks during fabrication and use severely limit the nanometer-scale patterns possible. Here, we used a periodic optical field instead of a physical mask to localize Ar* atoms on a nanometer length scale. A single infrared (IR) standing-wave field was used both to de-excite atoms from the metastable state to the inert ground state and to confine the remaining metastable atoms in an optical potential. The metastable atoms were quenched to the atomic ground state everywhere except in narrow regions around the nodes of the standing wave. The resulting center-of-mass wave packets occupied primarily the lowest vibrational bound state of the optical potential. The product of the widths of the transverse position and momentum distributions of metastable atoms transmitted through each node approached the limit stated by the Heisenberg uncertainty principle.

A variety of indirect methods have been used previously to probe the atomic localization induced by optical fields. Unlike the spectroscopic (*7*, *8*), time-of-flight (*9*), and state-selective transmission (*10*, *11*) techniques demonstrated elsewhere, the method presented here directly probes the atomic distribution as it strikes the surface. The length scale of these spatial distributions of atoms was much smaller than the diffraction limit of the optical pumping light. The demonstrated resolution (~0.02 μm) (*4*) of the pattern transfer techniques is high enough to allow the spatial imaging of the low-lying states of atoms in a simple harmonic oscillator (SHO) potential.

A simplified argon level structure that allows the formation of patterns by optical pumping is shown in Fig. 1. Metastable atoms $|m\rangle$ can be excited to a higher lying excited state $|e\rangle$ by laser light (801.479 nm). The laser field drives the $|m\rangle \rightarrow |e\rangle$ transition with an interaction strength characterized by a Rabi frequency, $\Omega$, and is detuned from the atomic resonance frequency, $\omega_0$, by $\delta = \omega_{laser} - \omega_0$, where $\omega_{laser}$ is the frequency of the laser. Atoms in $|e\rangle$ can radiatively decay back to the atomic ground state $|g\rangle$, dissipating the atom's internal energy as an ultraviolet (UV) photon. The excited state decays at a total rate $\Gamma$, and the atoms decay with probability $\Lambda$ to $|g\rangle$, and with probability $1 - \Lambda$ back to $|m\rangle$. Repeated excitations and spontaneous decays will optically pump all of the metastable atoms to $|g\rangle$, a process termed "optical quenching." Once the atoms have returned to the ground state, they do not have enough energy to affect the surface.

We used a one-dimensional (1D) standing wave (Fig. 2A) to pattern a beam of Ar* by optical quenching and then used the resulting pattern to deposit a carbonaceous film on a substrate. When $\Lambda$ is near unity, we can neglect the effect of atoms returning to the metastable state after a spontaneous emission. Even when $\Lambda$ is not near unity, for a laser-atom interaction of sufficient strength and interaction time, atoms traveling through the laser light are quenched with sufficiently high probability that metastable atoms are transmitted only in narrow regions of near-zero field around the intensity nodes. This "virtual" absorption grating produces high contrast in the metastable population transmitted at the nodes relative to the antinodes because the metastable population undergoes fast exponential decay in the high-field regions. We use the term "virtual" to indicate that the atoms are effectively removed because of a change in their inter-

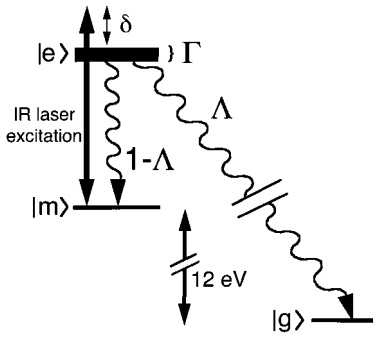


**Fig. 1.** Simplified diagram of the argon level structure used in the experiment. An IR laser photon can excite the atom from the metastable state $|m\rangle$ ($4s[3/2]_{J=2}$, $m_J = 2$) to an excited energy state $|e\rangle$ ($4p[5/2]_{J=2}$, $m_J = 1$) that can radiatively cascade back to the atomic ground state $|g\rangle$, dissipating the internal energy of the metastable state (12 eV) as a UV photon and rendering the atom unable to change material on a surface. See text for discussion of variables $\delta$, $\Gamma$, and $\Lambda$.

Department of Physics, Harvard University, Cambridge, MA 02138, USA.

*Present address: IGEN International Inc., 16020 Industrial Drive, Gaithersburg, MD 20877, USA.
†Present address: MIT Lincoln Laboratory, Analog Device Technology Group, Lexington, MA 02173, USA.
‡Present address: Lehman Brothers, 3 World Financial Center, New York, NY 10285, USA.

nal state, but are not physically removed from the distribution. Localized regions of transmission with widths ~λ/25 and contrasts of ~100:1 to 1000:1 are predicted by fully quantum-mechanical calculations for a variety of realistic experimental situations (*12*). This high-contrast, subwavelength localization results directly from the nonlinearities of the de-excitation process.

To understand fully the resulting pattern, it is necessary to consider both the diffraction of the matter waves and the forces exerted on the atoms by the optical field. As the distribution of Ar* atoms becomes spatially localized, it begins to diffract. During the optical pumping time required to achieve high-contrast localization, this diffraction causes the atoms to move away from the nodes, enter regions of higher laser intensity, and begin to quench rapidly. The effects of diffraction can be offset, however, if the atoms are confined to the nodal regions by an external force. This confinement was achieved by detuning the laser frequency above the atomic resonant frequency so that Ar* atoms adiabatically entering the standing wave experienced a potential with minima at the standing-wave nodes. As the quenching process increasingly localizes the Ar* atoms at the nodes, the time evolution of the spatial distribution of the metastable atoms is best described in terms of the quantized energy levels of the optical potential wells.

The quantum-mechanical mode structure of the standing-wave potential near a node, including the three lowest energy levels and their corresponding energy eigenfunctions, is shown in Fig. 2B. For sufficiently far detuned laser fields ($\delta > \Gamma$), the SHO nature of the confining potential near the nodes permits analytic expressions for quantities such as the state-dependent decay rate $\gamma_n$, the width of the position distribution $\delta x$, the width of the momentum distribution $\delta p_x$, and the oscillation frequency $\omega_{osc}$. Calculations can be simplified by ignoring the effect of spontaneously emitted photons and by assuming a low degree of atomic excitation near the nodes. Adiabatic elimination of the excited state allows the replacement of a full master-equation treatment with an ef-

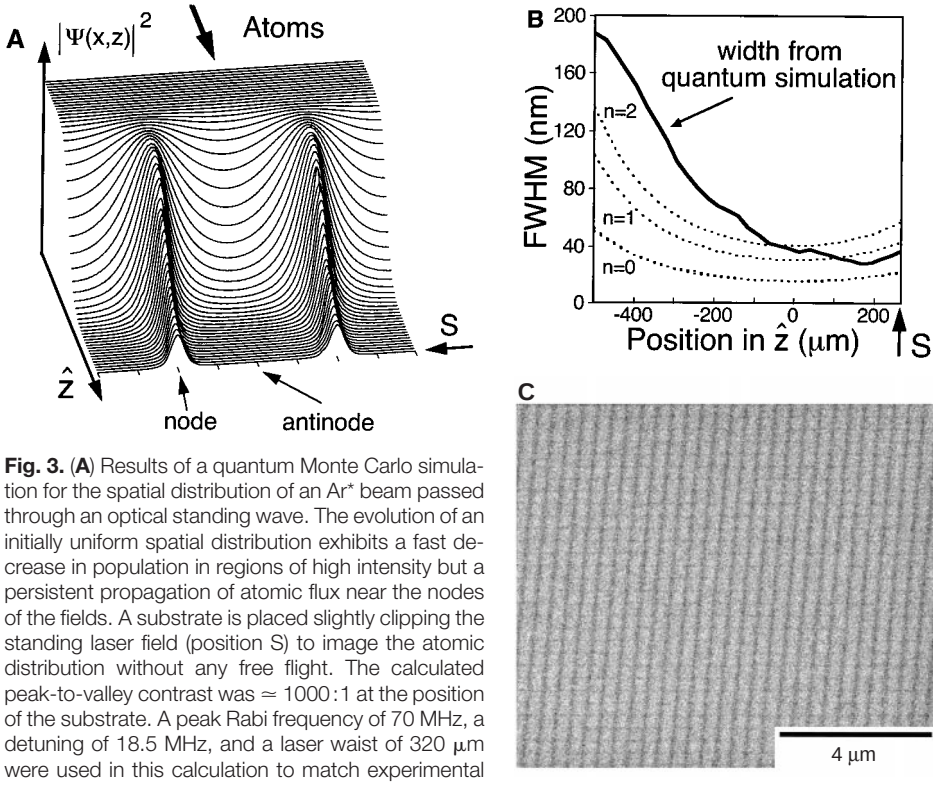


**Fig. 3.** (**A**) Results of a quantum Monte Carlo simulation for the spatial distribution of an Ar* beam passed through an optical standing wave. The evolution of an initially uniform spatial distribution exhibits a fast decrease in population in regions of high intensity but a persistent propagation of atomic flux near the nodes of the fields. A substrate is placed slightly clipping the standing laser field (position S) to image the atomic distribution without any free flight. The calculated peak-to-valley contrast was ≃ 1000:1 at the position of the substrate. A peak Rabi frequency of 70 MHz, a detuning of 18.5 MHz, and a laser waist of 320 μm were used in this calculation to match experimental parameters for the deposition shown in (C). (**B**) The evolution of the FWHM of the position distribution shown in (A) illustrates the localization induced by the optical pumping. Dotted lines indicate the widths of the three lowest vibrational states of the potential well. (**C**) An SEM image of material deposited on a silicon dioxide substrate exposed for 8 hours to an atom beam transmitted through a standing wave, as described above.

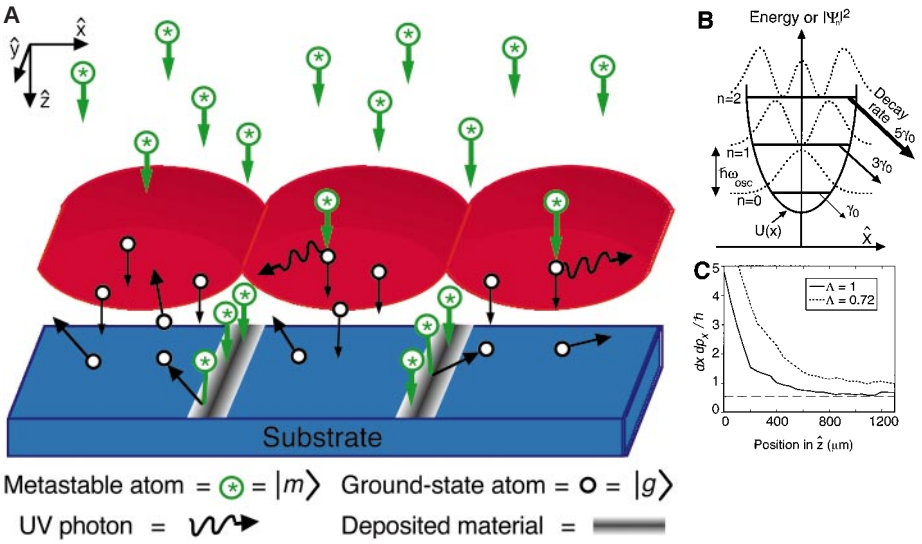


**Fig. 2.** (**A**) Schematic diagram of the spatially dependent optical pumping used to create wave packets limited only by the matter wave diffraction. The atoms are optically quenched everywhere except in narrow regions around the nodes of the standing wave. The transmitted metastable atoms interact with the surface and a background vapor precursor (not shown) to deposit a carbonaceous material. (**B**) The first three quantized vibrational energy levels (solid) and energy eigenfunctions (dotted) of the harmonic potential, $U(x)$, that is formed near the nodes of the standing-wave laser field. The atoms populating higher energy levels are optically pumped more rapidly because they extend further into regions of high light intensity. (**C**) The product of the spread in the transverse momentum and position widths calculated in a quantum Monte Carlo simulation shows the approach to the minimum uncertainty wave packet. A minimum uncertainty product of $\hbar/2$ (dashed line) is characteristic of the lowest bound state of a harmonic potential. Theoretical results are shown for an idealized quenching probability ($\Lambda = 1$, solid line) and the actual quenching probability for Ar* ($\Lambda = 0.72$, dotted line). The results are for argon atoms at 800 m $s^{-1}$, initially collimated to 0.3 mrad (full width) in the transverse direction. The atoms interact with a laser profile that turns on slowly and is then held constant at a peak Rabi frequency of 100 MHz and a detuning of +30 MHz.

fective Hamiltonian that is valid near the nodes

$$H_{\text{eff}} = \frac{p_x^2}{2M} + \hbar \frac{s_0}{2} (k_{\text{laser}} x)^2 \left( \delta - i\Lambda \frac{\Gamma}{2} \right) |m\rangle\langle m| \quad (1)$$

(*13*), where $s_0 = \Omega^2/[2(\delta^2 + \Gamma^2/4)] \gg 1$ is the peak saturation, $\Gamma$ is the natural linewidth of $|e\rangle$, $k_{\text{laser}} = 2\pi/\lambda_{\text{laser}}$ is the wave vector of the quenching light, M is the mass of the atom, and $\hbar$ is Planck's constant divided by $2\pi$. Near the nodes of the standing wave, the laser field forms nearly SHO potential wells, in which the energies of the lowest bound states are given by $E_n = (n + 1/2)\hbar\omega_{\text{osc}}$, where $n$ is the level number, $\omega_{\text{osc}} = (\omega_{\text{rec}}\Omega^2/\delta)^{1/2}$ is the oscillation frequency, and $\omega_{\text{rec}} = \hbar k_{\text{laser}}^2/2M$ is the atomic recoil frequency. The quenching rates $\gamma_n$ of the low-lying levels increase with well state number as $\gamma_n = 2(n + 1/2)\gamma_0$ (*14*), where $\gamma_0 = 1/4 s_0 \Lambda\Gamma(\omega_{\text{rec}}/\omega_{\text{osc}})$. Because the excited well states decay more rapidly than the lowest vibrational state, only the lowest state will be substantially populated after a sufficient interaction time $\tau_{\text{int}}$. If we assume that the initial distribution of population in the harmonic well states is uniform, the population of the well states appears to be thermally distributed during its evolution (because of the linear dependence of quenching rate on level number). This corresponds to a 1D effective temperature that decreases as $(\gamma_0\tau_{\text{int}})^{-1}$ to an ultimate value of ~1 μK. The rapidly decreasing effective temperature cannot be described as "cooling" because it results only from the preferential removal of hot atoms, not from energy removal from the remaining metastable atoms.

The effect of the random nature of spontaneously emitted photons on the atomic evolution can be included by using a quantum Monte Carlo simulation (*15*). The simulated evolution of the product of the transverse root-mean-square position and momentum distribution of an ensemble of atoms traveling through a standing wave is shown in Fig. 2C. The uncertainty product, $\delta x \delta p_x$, for both the ideal quenching probability, $\Lambda = 1$, and the actual quenching probability of Ar*, $\Lambda = 0.72$, is shown. When all of the atoms undergoing a single spontaneous emission are pumped to the ground state ($\Lambda = 1$), the distribution asymptotically approaches the minimum uncertainty product of $\hbar/2$, which corresponds to pure occupation of the lowest bound state of the system. However, the recycling of atoms back into the metastable manifold ($\Lambda < 1$) prevents the uncertainty product from reaching $\hbar/2$ because the atoms have a finite probability of returning to excited vibrational levels or to a strong-field-seeking state in which the potential does not confine the atom near the node. Still, as shown in Fig. 2C, the physical properties of Ar* ($\Lambda = 0.72$) allow the uncertainty product to fall well below the first-excited-state value of $3/2\hbar$. If we assume that the atoms are thermally distributed, this value corresponds to ≥50% of the atoms populating the ground state of the potential well. By correlating the ground-vibrational (external) state of the atom in the potential well with the internal energy state ($|m\rangle$) of the atom, we can image the spatial extent of the lowest vibrational level.

In our experiment, Ar* atoms were collimated by two stages of laser cooling, prepared in a well-defined initial atomic state, and then passed through the standing-wave laser field (*16*). The calculated spatial distribution of atoms across a single optical wavelength as it evolves in the optical field is shown in Fig. 3A. This quantum Monte Carlo calculation used the experimental laser beam and atom beam parameters designed to create ground-state distributions. A substrate was placed clipping the standing laser field to image the atomic distribution while the atoms were still confined in the optical potential (*17*). Figure 3B depicts the full width at half maximum (FWHM) spatial widths of the calculated distributions shown in Fig. 3A. Also shown are the widths of the three lowest bound states, calculated analytically in the SHO approximation (*18*). Atoms traveling at the most probable velocity were calculated to have a position distribution with a width just 25% greater than the width of the lowest bound state when they hit the substrate.

Figure 3C shows a scanning electron microscopy (SEM) image of the carbonaceous material deposited in the experiment (*19*) described in Fig. 3, A and B. The height of the lines of carbonaceous material deposited onto the surface was 0.6 ± 0.3 nm, as measured by atomic force microscopy (AFM) (*20*). The imaging of the deposited material can provide the most direct information about the spatial distribution of the atoms, because there is a linear relation between atomic dose and deposited material thickness (*4*). However, larger atomic doses are needed to extract reliable quantitative information from these images.

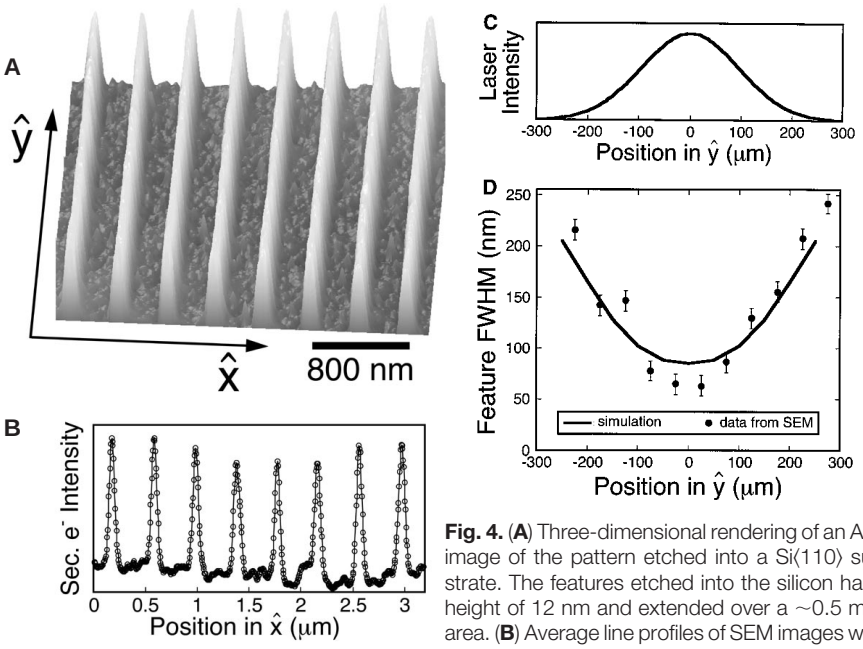


**Fig. 4.** (**A**) Three-dimensional rendering of an AFM image of the pattern etched into a Si⟨110⟩ substrate. The features etched into the silicon had a height of 12 nm and extended over a ~0.5 mm² area. (**B**) Average line profiles of SEM images were used to determine the width of the features. Analysis of the secondary electron intensity versus position indicates that the FWHM of the lines is 65 ± 5 nm. (**C**) The peak laser intensity is shown as a function of position in the $\hat{y}$ direction. (**D**) The measured width of the lines etched into the substrate shown in (A) and the calculated widths for the transmitted metastable distributions are shown as a function of position. A laser power of 2.25 mW, laser detuning of 28 MHz, and laser waist of 180 μm were used for the atom beam patterning. The measured FWHMs were determined by analyzing SEM images and were typically averaged over ~0.5 μm along the direction of the lines. Theoretical widths are FWHMs calculated by a quantum Monte Carlo simulation for measured experimental parameters. The $\hat{y}$ origin was used as the only free parameter to fit the data and theory. This comparison shows that this patterning technique provides quantitative information about distributions formed in atom optics experiments on the sub-0.1-μm length scale.

Further enhancements in the incident atomic dose or in the efficiency of the resist formation process should produce better direct images.

A development stage was used to enhance the contrast of the images; this procedure improved the images sufficiently to allow the extraction of quantitative information from the exposures. We developed the images by using a variety of wet and dry chemical etching techniques to transfer the patterns formed in the carbonaceous material into the substrate (*21*). Figure 4A shows a 3D rendering of an AFM image (*22*) of 12-nm-tall features, etched into a Si⟨110⟩ substrate after exposure (*23*) to a patterned Ar* beam. Figure 4B shows an integrated line profile of an SEM image of the features formed in the same exposure as those shown in Fig. 4A. Analysis of this profile indicated that the features have a FWHM of 65 nm; this width is consistent with the AFM measurements, given the expected broadening of the image as a result of the AFM tip width. In this exposure, a pattern of distinct lines was transferred into the substrate over an area of ~0.5 $mm^2$.

The quenching laser beam had a cylindrically symmetric Gaussian intensity profile. Atoms crossing the laser beam away from the axis experienced a peak laser intensity that was less than the maximum peak intensity. By measuring the widths of the etched lines as a function of their position in the $\hat{y}$ direction on the substrate, we determined the relation between linewidth and peak laser intensity. We then compared these results with theoretical calculations.

Figure 4C shows a profile of the laser intensity as a function of position along the substrate ($\hat{y}$ direction in Fig. 4A). Figure 4D displays both the measured widths of the lines and the FWHM of the calculated atomic distributions as a function of position in the laser beam profile. This comparison of theoretical and experimental widths demonstrates the quantitative use of the resist-etch system as a high-resolution detector capable of probing the characteristics of the spatial distributions of metastable atoms on the sub-0.1-μm length scale.

In the technique described here, the spatial distribution of neutral atoms approaches a high-contrast, time-independent state whose width is limited only by the quantum-mechanical diffraction of matter waves. In contrast, lithographic techniques using standing-wave light fields to focus atom beams (*24, 25*) have feature sizes and peak-to-valley contrasts limited by source and lens aberrations, and the localization is maintained only over a finite depth of focus. Furthermore, the lower power requirements and longer time scale of optical pumping (relative to focusing) allow the use of larger laser beams with less nodal curvature, which is ideal for precision submicrometer metrology; the pattern exhibits excellent long-range registration with an absolute accuracy referenced to atomic frequency standards. If metastable xenon (Xe*) were used in a similar experiment, calculations show that features with widths of ~10 nm (FWHM) are possible because of the greater mass of Xe*. Because the spatially dependent optical pumping relies only on the existence of nodes in a spatial interference pattern of laser light of an appropriate wavelength, these patterning techniques can also be extended to more arbitrary patterns [such as 2D standing waves (*26*)] created through holographically produced nodal patterns (*27*), where the local atomic distribution can approach the lowest vibrational state for each node.

## REFERENCES AND NOTES


1. Argon atoms in the $4s[1/2]_{J=0}$ and $4s[3/2]_{J=2}$ states have 11.72 and 11.55 eV of internal energy, respectively. Their natural lifetimes are both ≥30 s, which is much longer than their flight time through the apparatus. Other noble gas atoms that have energetic metastable states and level structures suitable for optical quenching experiments are Ne (17 eV), Kr (10 eV), and Xe (8 eV). In this experiment the $4s[3/2]_{J=2}$ state was used.
2. The transfer of energy to the hydrocarbon molecules is localized to less than 1 nm, which is ideal for high-resolution detection. See Y. Harada, S. Masuda, H. Ozaki, *Chem. Rev.* **97**, 1897 (1997), and references therein.
3. K. S. Johnson *et al*., *Appl. Phys. Lett.* **69**, 2773 (1996).
4. J. H. Thywissen *et al*., *J. Vac. Sci. Technol.* **16B**, 1155 (1998).
5. S. J. Rehse *et al*., *Appl. Phys. Lett.* **71**, 1427 (1997).
6. K. K. Berggren *et al*., *Science* **269**, 1255 (1995); S. Nowak, T. Pfau, J. Mlynek, *Appl. Phys. B* **63**, 203 (1996).
7. M. G. Prentiss and S. Ezekiel, *Phys. Rev. Lett.* **59**, 2631 (1987); C. Salomon, J. Dalibard, A. Aspect, H. Metcalf, C. Cohen-Tannoudji, *ibid.,* p. 1969.
8. P. S. Jessen *et al*., *ibid.* **69**, 49 (1992).
9. T. Müller-Seydlitz *et al*., *ibid.* **78**, 1038 (1997).
10. J. E. Thomas and L. J. Wang, *Phys. Rep.* **262**, 311 (1995) and references therein.
11. R. Abfalterer *et al*., *Phys. Rev. A* **56**, R4365 (1997).
12. A. P. Chu, K. K. Berggren, K. S. Johnson, M. G. Prentiss, *Quantum Opt.* **8**, 521 (1996).
13. C. Cohen-Tannoudji, J. Dupont-Roc, G. Grynberg, *Atom-Photon Interactions* (Wiley, New York, 1992).
14. These decay rates $\gamma_n$ can be calculated perturbatively when $\gamma_0 < \omega_{osc}$ (that is, when the vibrational levels are well resolved).
15. J. Dalibard, Y. Castin, K. Molmer, *Phys. Rev. Lett.* **68**, 580 (1992).
16. The dc discharge source emits ions, electrons, photons, ground-state atoms, and atoms in both the $4s[1/2]_{J=0}$ and $4s[3/2]_{J=2}$ metastable states. Atoms in the $J = 0$ level were optically quenched using a 794.82-nm laser beam. The ions and electrons were removed from the beam by electrostatic deflection. The atom beam was laser-cooled by an 811.53-nm laser beam detuned slightly below the $4s[3/2]_{J=2} \rightarrow 4p[5/2]_{J=3}$ closed transition in a 5-cm-long interaction region. This cooling zone was placed as close to the source as possible, both to collimate the beam and to enhance the flux density that reached the sample region. A quantizing magnetic field of ~1 G, parallel to the laser propagation direction ($\hat{x}$), was applied in the sample region. Immediately before the standing-wave quenching interaction, a second laser cooling region of right circularly polarized light further reduced the transverse temperature of the atom beam and optically pumped the atoms to the $J = 2$, $m_J = +2$ magnetic sublevel. We used left circularly polarized quenching light in our experiments to excite the $m_J = +2 \rightarrow m_J = +1$ transition. These laser polarizations reduced the complex, multilevel state structure to the simplified level structure described in this report. In our calculations, we ignore the role of atoms returning to a different magnetic substate of the $J = 2$ manifold, as these atoms have a small effect on the spatial distributions produced.
17. Because of the diffraction of the laser beam from the edge of the substrate and experimental misalignments, the standing wave must suffer some imperfection immediately above the substrate. The extent of the clipping and the distance from the front edge of the substrate to the mirror are sufficiently small that we can neglect these contributions to the free flight experienced by the atoms.
18. The widths calculated numerically for the actual atom-laser potential agreed with the analytic predictions for these low well states, justifying the use of the SHO approximation in this regime.
19. The substrate was exposed for 8 hours to the atom beam patterned by a standing wave with a waist ($1/e^2$ half width) of 320 μm, power of 7.5 mW, and detuning of 18.5 MHz. During this long exposure, the temperature of the mount holding the substrate and the mirror used to generate the standing wave was stabilized to ±30 mK to ensure that the substrate did not move relative to the nodes of the standing wave. The sample mounting system was affixed rigidly inside the vacuum system and was designed for a high degree of passive mechanical stability.
20. Atomic force microscope imaging was performed in contact mode on a Park Scientific AFM.
21. Isotropic wet chemical etches and anisotropic dry chemical etches were both used to transfer standing-wave quenching patterns into substrates. Ferricyanide was used to etch into gold, a two-step 1% HF/alcoholic KOH solution was used for Si⟨110⟩ and Si⟨100⟩ substrates, and reactive ion etching with $CF_3$ was used for silicon dioxide substrates.
22. Using the measured signal-to-noise ratio in the regions between the features as an input parameter, we applied a Weiner filter to the data shown to reduce the effects of measurement noise.
23. The substrate was exposed for 5 hours to a beam of Ar* patterned by a standing laser field with a waist of 180 μm, power of 2.25 mW, and detuning of 28 MHz. The deposited carbonaceous material was used as a mask to protect against an aqueous 1% HF etch that removed the native oxide layer. A subsequent 70°C alcoholic KOH solution was used to transfer the pattern into the underlying silicon substrate.
24. R. E. Behringer, V. Natarajan, G. Timp, *Appl. Phys. Lett.* **68**, 1034 (1996).
25. J. J. McClelland, R. E. Scholten, E. C. Palm, R. J. Celotta, *Science* **262**, 877 (1993).
26. R. Gupta, J. J. McClelland, Z. J. Jabbour, R. J. Celotta, *Appl. Phys. Lett.* **67**, 1378 (1995); U. Drodofsky *et al*., *Appl. Phys. B* **65**, 755 (1997).
27. In a demonstration of this potential for arbitrary pattern formation, the optical diffraction pattern formed by quenching light diffracting through a 10-μm-wide slit was used to pattern an Ar* beam [K. K. Berggren, thesis, Harvard University (1997)].


28. Supported in part by NSF grant PHY 9312572. This work made use of the Harvard–Materials Research Science and Engineering Center (NSF) shared facilities. K.S.J. was supported by an AT&T/Lucent Technologies Graduate Fellowship. J.H.T. was supported by the Fannie and John Hertz Foundation.

4 February 1998; accepted 13 April 1998